Post-Print

Louis Gagnon provides this scientific self-archived article free of charge.
For more research info see LouisGagnon.com

This article is the final submission, post-review, version of the following article:

RESEARCH ARTICLE

An overview of various new road profile quality evaluation criteria : part 2

Louis Gagnon,[a*] Guy Doré,[b]

and Marc J. Richard[a]

[a]*Department of Mechanical Engineering, Laval University, Québec, QC, Canada*;
[b]*Department of Civil Engineering, Laval University, Québec, QC, Canada*

(*Submitted for review*)

This is the second part of an article which correlates road induced impacts on vehicle to a selection of road assessment criteria. The impacts on tyre, suspension, and radiator wear are studied by running a multibody semitrailer truck model on 270 road profiles. The model accurateness is assessed by comparing IRI-impact relationships to the literature. A new profile rating method uses wavelength content to predict the various impacts of a specific profile. It is concluded that 1) medium wavelengths severely impact fuel consumption, component wear, and safety; 2) simple, two point, and four point indices yield similar results, but the more points the better the correlation; and, 3) the IRI is good at predicting general trends in road-induced vehicular impact but is weak for specific impacts 4) tyre wear correlates linearly while component wear requires quadratic correlations.

Keywords: road roughness; IRI; quarter car; fatigue; vehicle wear; wavelength)

1.   Introduction

It is a well known fact that irregular road surfaces stress the vehicles which operate on them. In fact, Zaniewski and Butler (1985) showed that the increase in vehicle operating costs on a degraded road surface was 80 times greater than the cost of restoring the road. Many reports also link poor road quality to substantial consequences on vehicle wear (FAA 2009, Rakheja *et al.* 2001, Howe *et al.* 2004).

Bearing that in mind, a number of authors have tested different approaches relating vehicle wear and road surface quality. In this paper, the wear of the tyres, suspensions,

*Corresponding author. Email: louis.gagnon.10@ulaval.ca

L. Gagnon, G. Doré, and M. J. Richard

and radiator is calculated using data obtained from the multibody model illustrated in Figure 1. That model was constructed with the sole purpose of measuring the impact road surface deformations have on the efficiency of a vehicle and has been used to individually test 270 longitudinal road profiles.
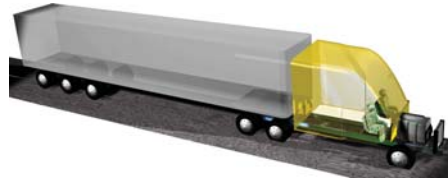

Figure 1. Schematic representation of the constructed multibody model.

Suspension and tyre wear are commonly examined in road-vehicle interaction research. Suspension damage is regularly estimated by fatigue analyses (Wetzel 1977, Conle and Mousseau 1991, Poelman and Weir 1992, Bogsjö 2006, Lin *et al.* 2006, Breytenbach and Els 2011, Yang and Xu 2012). In fact, Rice (1997) reports that more than 60% of the failures in construction vehicles are caused by fatigue. As for the numerical evaluation of tyre wear, frictional energy is often relied upon (Savkoor 1966, Zaniewski and Butler 1985, Veith 1986, Knisley 2002, Aukland *et al.* 2003, Cho *et al.* 2011). Hence, fatigue and frictional energy analyses were selected to evaluate suspension and tyre wear, respectively. The suspensions were evaluated by looking at the accumulated damage computed from an uniaxial fatigue analysis taking dynamic forces as input. Tyres were evaluated by computing frictional energy from the slip forces and contact patch velocities.

Nevertheless, the components of a vehicle in operation are subjected to multiaxial stresses. These require a different treatment in the evaluation of fatigue. A popular approach is to rely on von Mises stresses, which are evaluated for each position of the component likely to have the highest accumulated fatigue (Preumont and Piéfort 1994, Pitoiset *et al.* 1998, Pitoiset 2001, Lee and Barkey 2012). Another approach is to find the most damaging of a multitude of hypothetical stresses which are made up from different combinations of the external forces acting on the part of interest (Pitoset *et al.* 1999, Bogsjö 2007). Quite often, fatigue analyses are even performed on components with know geometries and for which a finite element analysis is used to identify which stresses contribute most to fatigue (Conle and Mousseau 1991, Pitoset *et al.* 1999, Saga *et al.* 2005, Lee *et al.* 2007, Rahman *et al.* 2008).

Thus, to further evaluate truck wear, an estimate of the multiaxial damage on radiator brackets is measured. This estimate is derived from a calculation which estimates the stresses from the radiator forces which have the greatest impact on radiator damage. The geometry used is simple and hypothetical and for this reason the results have to be considered as informative but not authoritative. Hence, while the suspension fatigue calculation method chosen is concordant with the literature on vehicle-profile wear studies, the radiator damage calculation is an improvement of the method inspired from what is done for different fatigue evaluation methods in other areas.

For both suspension and radiator damage, a quasi static damage accumulation analysis is used. It is a common approach (Haiba *et al.* 2002) deemed appropriate for vehicle wear calculation (Breytenbach and Els 2011).

Finally, in order to supplement the analysis conducted in part 1 of this paper, a profile wavelength analysis method was also developed. It consists of estimating the likelihood of a wavelength at a specific amplitude to foretell of a specific impact. Whenever short,

medium, and long wavelengths are mentioned in this paper, they are the bandwidths from 0.707 m to 2.83 m, 2.83 m to 11.3 m, and 11.3 m to 45.2 m, respectively and as designated by Martel *et al.* (2011).

2.   Technical approach

This section summarises the methodology used to model the vehicle, run it on a profile, evaluate the impact on the vehicle, and characterise the different profiles.

2.1.   *Multibody model*

The tractor has a conventional cab and is coupled to a semitrailer van with three axles. This assembly is modelled with the open-source MBDyn software and the description which follows uses the software's lingo to allow the reader to reproduce the multibody model. Table 1 gives the definitions and symbols associated with the terms presented. Throughout this article the x-axis points to the front of the truck, the y-axis points to the left, and the z-axis points upwards.

Figures 2 to 12 graphically show the construction of the model in the MBDyn software of which Figures 2 to 5 focus on the different vehicle fragments. Elements L1 to L7 presented in those figures are then depicted in Figures 6 to 12. Finally, the symbols used in all those figures are explained in Table 1.
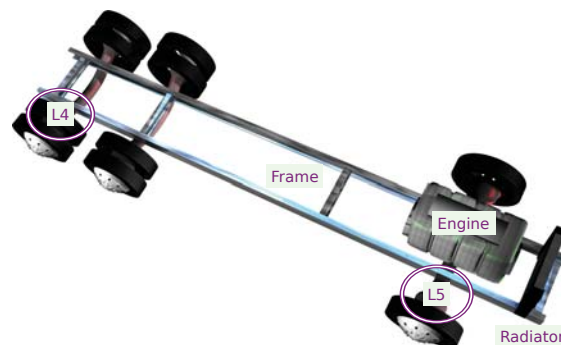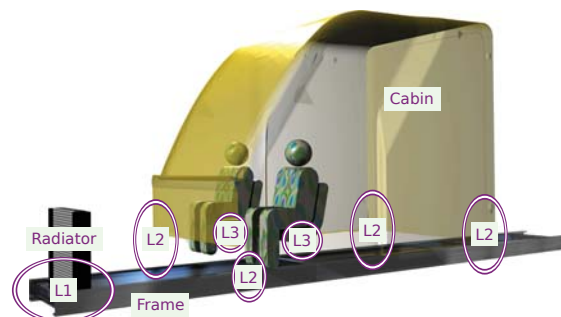

Figure 2. Tractor wheels.

Figure 3. Tractor cab.

L. Gagnon, G. Doré, and M. J. Richard

Table 1.   Identification of the multibody elements.

| Sym.	Element name	Description
C	revolute hinge joint	restrains any relative movement between two rigid bodies except for the rotation about one axis
E	in line joint	forces a point on one body to follow a line attached to a second body
G	centre of mass	in Figures 6 to 12 the centre of mass is connected to the elements when representative of the multibody model
H	cardano rotation joint	forces two bodies to maintain the same relative orientation about one of their axes
P	prismatic joint	forces two bodies to maintain the same relative orientation about all of their axes
R	revolute rotation joint	forces two bodies to maintain the same relative orientation about two of their axes
S	spherical hinge joint	forces points on two bodies to maintain the same relative position
T	total joint	allows to constrain DoF between two bodies based on user defined equations. In Figure 10, all DoF are blocked except for the rotation about the local vertical axis which is governed by a steering function
1	deformable displacement joint (viscoelastic)	applies a unidimensional rectilinear interaction force between two bodies which depends on stiffness and damping coefficients given by the user and the distance between those two bodies expressed in the coordinate system of one the two bodies
3	deformable displacement joint (viscoelastic)	applies a tridimensional rectilinear interaction force between two bodies which depends on stiffness and damping coefficients given by the user and the distance between those two bodies expressed in the coordinate system of one the two bodies
3'	deformable hinge joint (viscoelastic)	applies a tridimensional interaction moment between two bodies which depends on stiffness and damping coefficients given by the user and the relative angles between the two bodies expressed in the coordinate system of one the two bodies
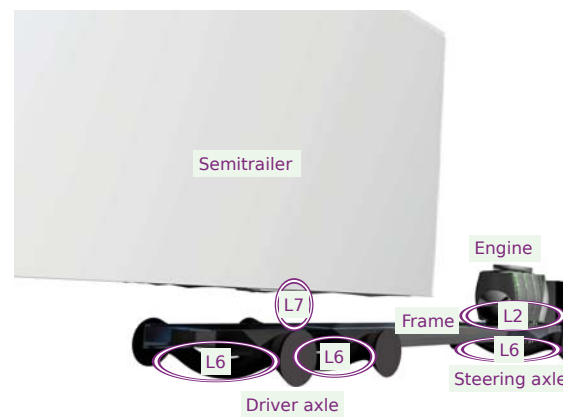
Figure 4. Tractor frame.

Because of the high complexity of the tyre model and the fact that the truck has 22 wheels, the multibody dynamics model ends up having 331 Degrees of Freedom (DoF). It represents each main component of the semitrailer truck by a mass. The tractor is a
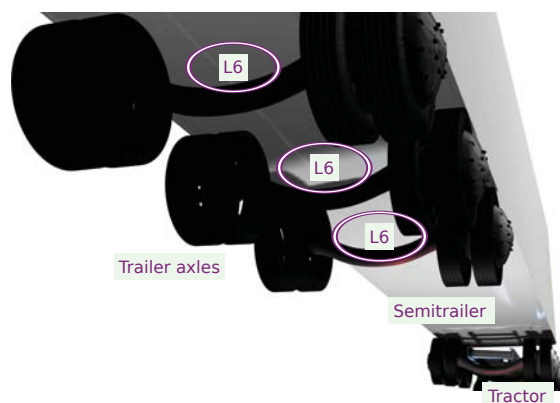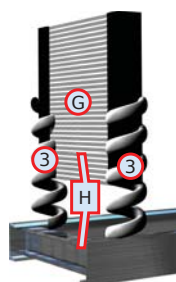
Figure 5. The semitrailer axles.

Figure 6. Exploded view of the L1 link between the frame and the radiator.

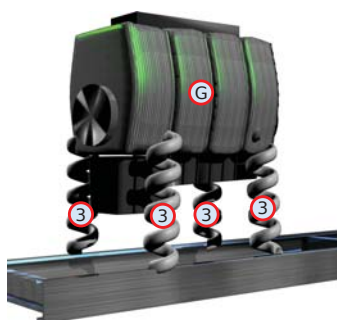Figure 7. Exploded view of the L2 link between the engine or the cab and the frame.
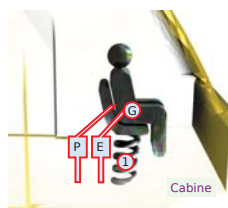

Figure 8. Exploded view of the L3 link between a passenger and the cab.

Freightliner Cascadia® and the trailer is a Manac® three axle van. This particular combination was chosen because it is a good representation of the typical trucks that travel on North American roads and the manufacturers agreed to provide essential technical
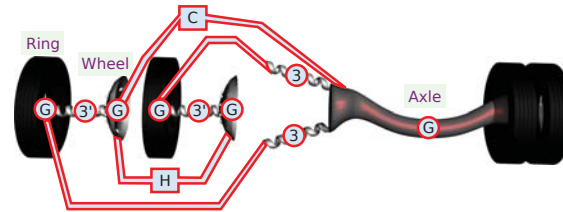
Figure 9. Exploded view of the L4 link between the dual wheels and their axle.
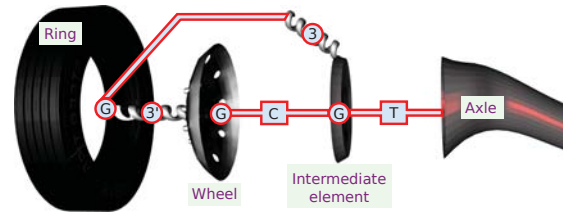
Figure 10. Exploded view of the L5 link between the steering wheels and their axle.
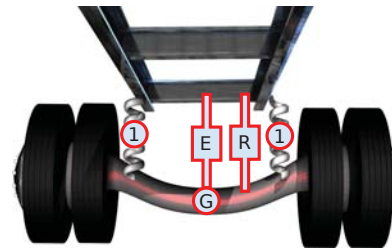
Figure 11. Exploded view of the L6 link between the axles and the tractor or the semitrailer.

Figure 12. Exploded view of the L7 link between the frame of the tractor and the semitrailer.

information specific to these vehicles. Energy losses in the various rotating parts of the vehicle are accounted for by functions dependent on their angular velocities. In addition to the wheels, 13 masses are used in the model, and they each have 6 DoF. There is one mass for each axle; one for the tractor chassis frame and components that are rigidly bond to it, such as the battery and fuel tanks; one for the engine; one for the cab; one for the driver and one for the passenger; one for the radiator; and, one for the trailer.

3.   Profile evaluation procedure

A profile evaluation study was conducted by running the developed truck model at 100 km/h in a straight line on two track longitudinal road profiles. The truck velocity was controlled by a custom cruise control algorithm which applies a torque to the drive wheels and produces a maximum of 306 kW (410 HP) minus 10% which are transmission losses. Two hundred and seventy 1 km road profiles sampled at 25 mm intervals on paved roads ranging from very smooth to very coarse were analysed. Both ends of each profile were padded in order to stabilise the vehicle before and after the test section.

3.1.   *Damage impact assessment*

First, the friction induced tyre damage $D_{\text{tyre},i}$ is obtained by,

$$D_{\text{tyre},i} = \sum |(\frac{\mathbf{x}_{\text{p},j+1} + \mathbf{x}_{\text{p},j-1}}{2} \cdot \mathbf{F}_j)| \tag{1}$$

for each tyre. The variable $\mathbf{x}_{\text{p},j\pm1}$ represents the position of the contact patch at timestep $j \pm 1$ and $\mathbf{F}_j$ the vector of the friction force between the tyre and the ground calculated at timestep j. The total tyre damage, D_{tyre}, is thus

$$D_{\text{tyre}} = \sum D_{\text{tyre},i} \tag{2}$$

Second, the fatigue damage, $D_{\text{susp},i}$ incurred by the suspension i, is computed by taking the vertical force that it withstands expressed is its local coordinate system as the stress $\sigma_{\text{s},i}$. Thus,

$$D_{\text{susp},i} = \sum_j ((2\sigma_{\text{s},j,i})^3 n_{\sigma_{\text{s},j,i}}) \tag{3}$$

where $n_{\sigma_{\text{s},j,i}}$ is the number of cycles for which the stress $\sigma_{\text{s},i}$ will have a magnitude $\sigma_{\text{s},j,i}$. These two values are obtained by a rainflow counting algorithm (Rychlik 1987, Lin *et al.* 2006). The sum of the damage incurred by all the suspensions together is thus,

$$D_{\text{susp}} = \sum_i D_{\text{susp},i} \tag{4}$$

This method of calculating the relative suspension damage by relying solely on one force component has been used by various authors (Poelman and Weir 1992, Bogsjö 2006, Breytenbach and Els 2011).

Third, the damage, D_{rad}, inflicted to the radiator by the vibrations is the maximum value between the accumulated fatigue contributions on the left and on the right brackets. An hypothetical radiator geometry is assumed and is shown on Figure 13 where the two pinpointed positions are the assumed maximum accumulated stress contribution. The forces and moments employed for the calculation are also depicted on the figure.

The moment contribution M_x is neglected because the points considered are on the neutral axis of the bending motion. A contribution in shear stress is taken into account and is caused by the moment about the y axis and the force in z. It is calculated according
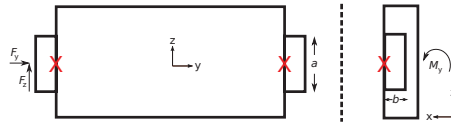
L. Gagnon, G. Doré, and M. J. Richard

Figure 13. Front and side views of the radiator and bracket geometry used for the fatigue calculation.

to the following equation,

$$\tau_{\mathrm{xz}} = \frac{F_{\mathrm{z}}}{ba} - \frac{M_{\mathrm{y}}r}{J} \tag{5}$$

where

$$J = \beta ab^3 \tag{6}$$

and where for the current geometry $a = 0.2$ m, $b = 0.08$ m, $r = \frac{b}{2} = 0.04$ m and $\beta = 0.249$. Then, another contribution comes from the lateral axial stress according to the following equation,

$$\sigma_{\mathrm{yy}} = \frac{F_{\mathrm{y}}}{ab} \tag{7}$$

Finally, the effective stress is calculated using the von Mises criteria as follows,

$$\sigma_{\mathrm{r},i} = \sqrt{\frac{1}{2}\sigma_{\mathrm{yy},i}^2 + 3\tau_{\mathrm{xz},i}^2} = \left((44.19 F_{\mathrm{y},i})^2 + (2717 M_{\mathrm{r},\mathrm{y}} + 108.3 F_{\mathrm{z},i})^2 \right)^{1/2} \tag{8}$$

where the index i identifies left and right brackets. The variable $M_{\mathrm{r},\mathrm{y}}$ is the y-component of the moment which keeps the radiator x-axis orthogonal to the tractor frame z-axis and $F_{\mathrm{y},i}$ and $F_{\mathrm{z},i}$ are the lateral and vertical components, respectively, of the force produced by the viscoelastic elements which attach the radiator to the tractor frame.

Once the stress formulae are known, the Basquin relationship is used, as shown by Bogsjö (2006), in the following equation,

$$D_{\mathrm{rad}} = \max_i \sum_j ((2\sigma_{\mathrm{r},j,i})^3 n_{\sigma_{\mathrm{r},j,i}}) \tag{9}$$

where $n_{\sigma_{\mathrm{r},j,i}}$ is the number of stress cycles of $\sigma_{\mathrm{r},i}$ which have a magnitude of $\sigma_{\mathrm{r},j,i}$ as measured by the rainflow algorithm.

In carrying this radiator damage analysis, it was assumed that the internal forces caused by acceleration act at the centre of mass and react to the bracket forces. The approach of trying every possible combination of the load was discarded because it disregards the geometry of the part and has a considerable processing time.

The accumulation approach used here for both suspension and radiator damage analyses are deemed especially useful by Preumont (1990) in performing comparative studies of fatigue, such as when accumulated damage under various conditions are compared against each other. It was also assumed that even though a mean stress may be present due to material pretension, it can be neglected because its effect will be to add a contribution to the accumulated damages, as presented by Boresi and Schmidt (2003). Thus,

identical pretensions give the same effect.

3.2.   *Road profile rating*

4.   **Results and trends identified**

For all the results presented, the indices were evaluated on 1 km road sections and the impacts were measured for a vehicle travelling at 100 km/h.

4.1.   *IRI verification*

The merit of the developed profile rating and impact calculation procedure was first confirmed by the relations between impact and IRI it yielded. Their linear correlations for the Qualified profile set are presented on Figures 14 to 18. Part 1 of this article exposed the profile sets definitions and the impact calculation methodology for criteria other than damage. Only linear correlations are presented because they have better coefficients of determination than the quadratic correlations.
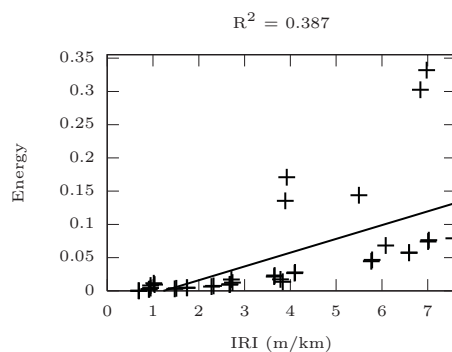
Figure 14. Linear correlation between normalised energy use and the IRI.

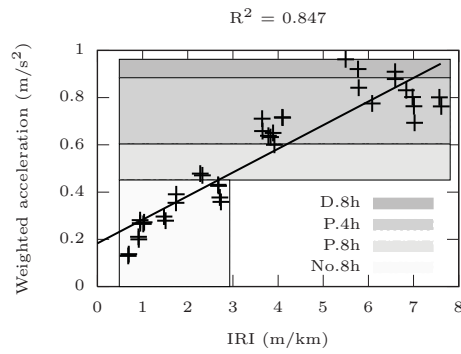   *L. Gagnon, G. Doré, and M. J. Richard*

Figure 15. Linear correlation between the impact on health and the IRI with delimiters for zones of danger (D), possible danger (P), and no danger (No) after continued daily exposures of 4h and 8h.
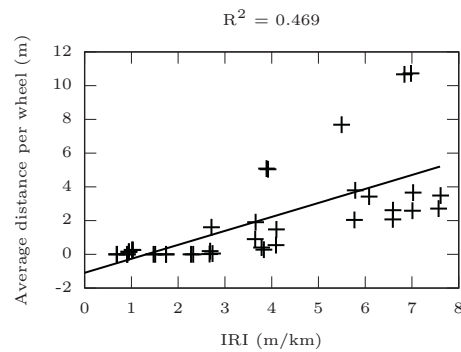

Figure 16. Linear correlation between the impact on safety and the IRI.
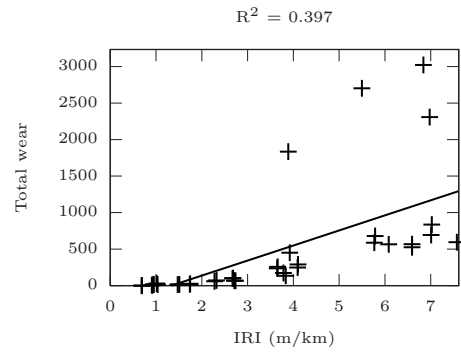

Figure 17. Linear correlation between the normalised impact on suspension wear and the IRI.
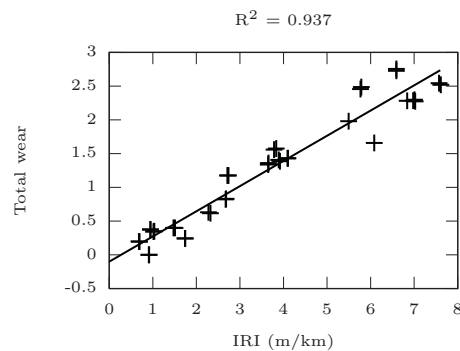
Figure 18. Linear correlation between the normalised impact on tyre wear and the IRI.

First, Figures 14 to 18 show that each impact will increase with the IRI, as shown in the literature. Then, the fuel consumption of Figure 14 agrees both with the 10% mean increase reported by Jackson *et al.* (2011) and the numerous studies reported by McLean and Foley (1998). Overall, the literature shows an important variation in the IRI-fuel consumption relationships and this is partly due to the fact that the IRI ignores wavelengths that do influence fuel consumption. Figure 15 agrees very well with the relationship found by Ahlin and Granlund (2002) which shows that the IRI to ISO-weighted acceleration at the floor of the Reference Quarter Car Simulation model travelling at 100 km/h is a linear monomial with a coefficient varying between 0.16 and 0.19. Furthermore, although not shown, the correlation obtained between driver discomfort at 100 km/h and IRI agrees quite well with IRI thresholds proposed by Cantisani and Loprencipe (2010) for comfort.

The zones of low adherence shown in Figure 16 correspond very well with what was shown by Richard *et al.* (2009) since zones with less than 30% contact force almost never appear for IRI below 3 m/km while such zones almost always appear for IRI above 5.5 m/km. Figure 17 agrees well with a study reported by Jones and Robinson (1986) which shows that truck operating costs will roughly double between IRI of 3 m/km and 7 m/km. The tyre wear calculated yields an excellent linear correlation and Figure 18 agrees with findings of Zaniewski and Butler (1985) who showed that, between a road in good and very bad states, tyre costs increase by 182% for trucks and 316% for cars and small trucks.

4.2.   *Wear*

The impact on vehicle tyre, suspension, and radiator wear is plotted in Figures 19 to 25 against a sample of the indices presented and explained in part 1 of this article. As a consequence of the normalisation procedure used for the graphics presented, the trends of Figures 19 and 20, Figures 21 and 22, and Figures 23 to 25, should not be compared in magnitude.

The results indicate that the Health and Wear indices are the most appropriate in evaluating impact on wear and that small and medium wavelengths affect wear significantly more than long wavelengths do. Also, if a short, medium, or long wavelength bandpass filter is applied to the profile before evaluation, the impact on wear diminishes.

The best suspension wear correlation is obtained from the Four point Health index, using a quadratic correlation, as shown on Figure 21. The Simple Health index, the FRI, and the IRI also allow reasonably good quadratic correlations with values of $R \sim 0.62$, $R \sim 0.48$, and $R \sim 0.41$, respectively. Quadratic correlations of the suspension wear are

L. Gagnon, G. Doré, and M. J. Richard
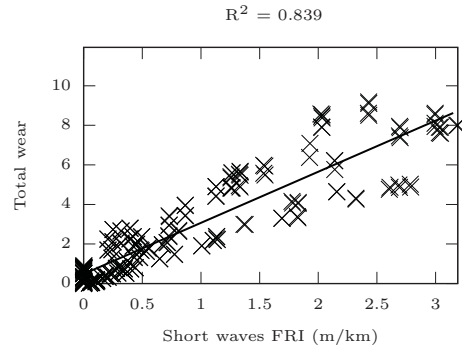

Figure 19. Linear correlation between normalised tyre wear and Short waves FRI.
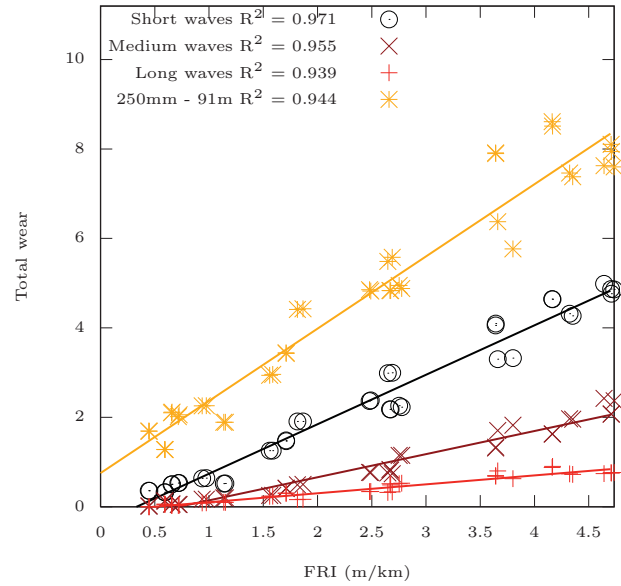

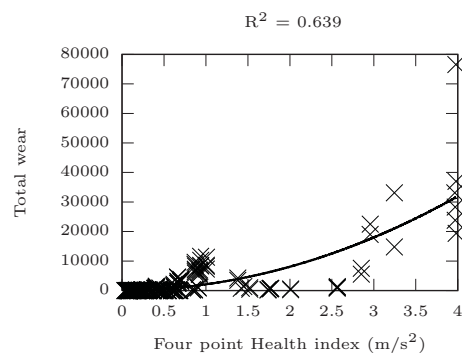Figure 20. Linear correlations between normalised tyre wear and FRI.

Figure 21.   Quadratic correlation between normalised suspension wear and the Four point Health index.
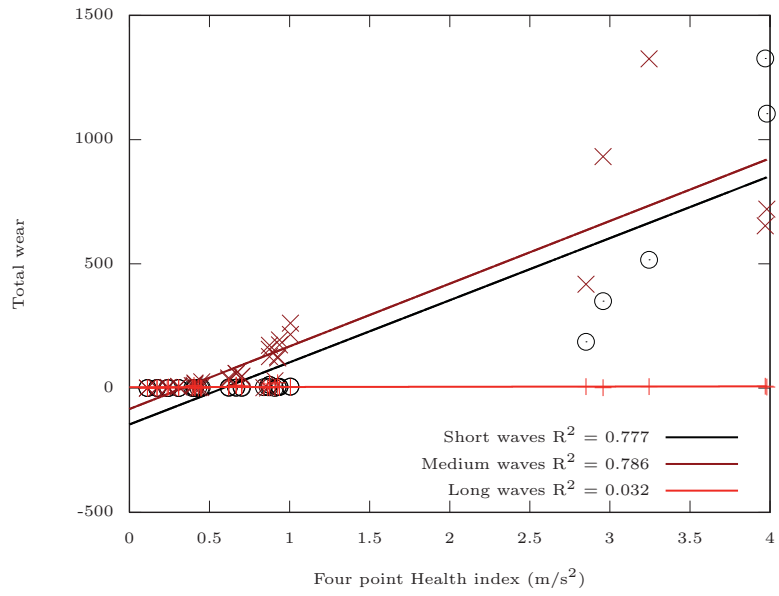
Figure 22. Linear correlations between normalised suspension wear and the Four point Health index.
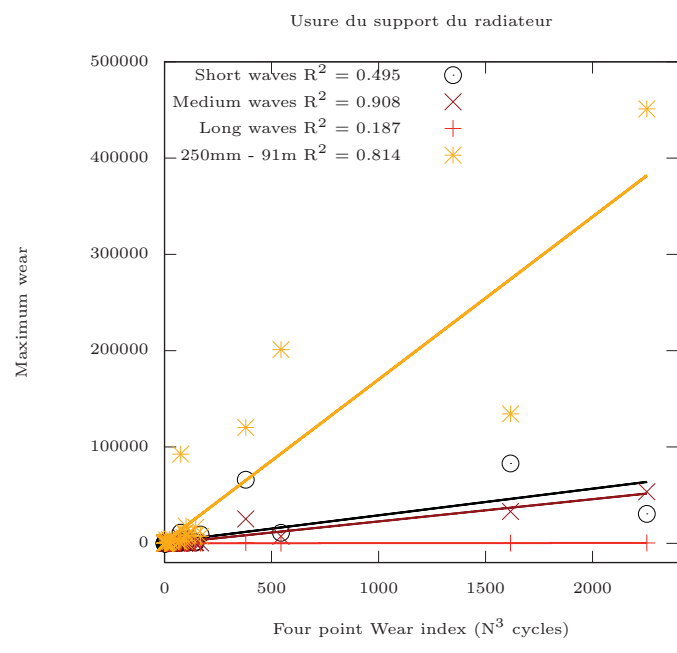
Figure 23. Linear correlations between normalised radiator wear and the Four point Wear index.

deemed sufficiently better to be used instead of linear ones. Precisely, the best linear correlation for suspension wear has $R^2 = 0.54$ while the best quadratic one reaches $R^2 = 0.65$. It is suspected, based on the good agreement between the Health index and wear, that the quality of the Wear index correlations would benefit from frequency weighting of the input signal.

L. Gagnon, G. Doré, and M. J. Richard

Figure 24.   Quadratic correlations between normalised radiator wear and the Simple Health index.
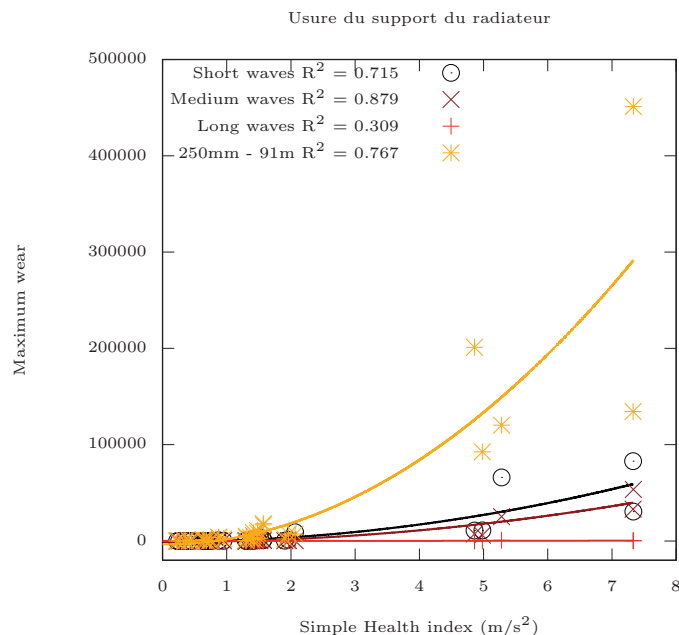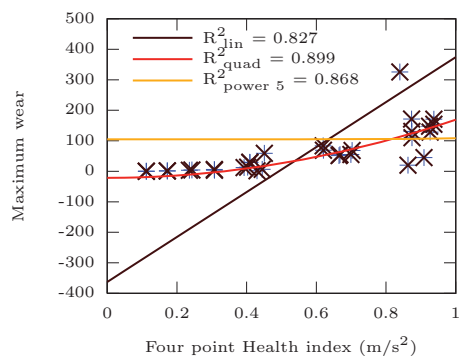

Figure 25.   Zoom on the low index values for the linear correlations between normalised radiator wear and the Four point Health index for the Qualified profile set.

Still for the suspension wear, the medium and long wavelengths had approximately equal impacts, as shown in Figure 22 where individual wavebands contributions are shown. It is also seen that if only one of these wavelengths of perturbation could be eliminated, the vehicle damage would reduce by 10 to 20 times. The quadratic correlation for the short waves with the Four point Health index had $R^2 = 0.91$. While many assumptions and simplifications were used in calculating vehicle wear, the results presented here do agree well with Howe *et al.* (2004) who found a 10,000 fold increase in damage when going from an IRI of 3 m/km to 3.3 m/km. Although this does not equate into costs, the accumulated damage is found to be 80,000 times greater for the worst profile evaluated than for the best one.

While the IRI does not show great suitability for predicting suspension wear, it does perform surprisingly well in predicting tyre wear, regardless of the fact that the *golden*

car does not allow any longitudinal tyre movement. The best correlation for the tyre wear is obtained from the Short waves FRI, as shown on Figure 19. Other indices that provide a good correlation are the Short waves HRI, the Short waves IRI, and the IRI, having $R^2 = 0.83$, $R^2 = 0.82$, and $R^2 = 0.81$, respectively. The wavelengths decomposition analysis shown on Figure 20 highlights the fact that the shorter the wavelength, the greater the tyre wear it can cause.

Figure 25 shows the radiator damage impact correlations using polynomials of different degrees and obtained from the unfiltered profiles. It is zoomed to focus on the low Health index values but the correlations presented come from data having index values between 0 m/s^2 and 4 m/s^2. The quadratic correlation offers the best agreement with the data, especially for the presented range. Finally, with values of $R^2 \sim 0.7$ the Safety index also yields an acceptable radiator wear correlation.

4.3.   *Wavelength analysis*

The size of the available dataset made it possible to produce graphs which classify profiles in terms of their wavelength content computed by the fast Fourier transform (FFT). In order to eliminate the null wavelength response, the mean profile height is subtracted from the signal prior to evaluating the FFT. The analysis yields a surface plot where each slot corresponds to a wavelength interval, an amplitude interval, and a measured impact and where the wavelength intervals are of 0.24 m, 1 m, and 3.77 m for the short, medium, and long wavelengths, respectively.

The procedure to obtain such a plot is as follows. First, the value of the impact contribution of each profile is added to every slot of the surface plot spanned by its FFT. Once all the profiles are taken into account, the slots of the graph are each divided by the total number of profiles in order to obtain average impact values.

The results plots are shown on Figures 26 to 32 which link the presence of wavelengths and amplitude combination to each impact category. The impacts are calculated as presented in this and in the previous part of the article. These plots give the presence of wavelengths and amplitudes combinations when specific impacts are provoked, but they refrain from assessing exactly which combination is the actual cause of the impact. Nevertheless, as the number of profiles used for such an analysis increases, the combinations that do not contribute to impacts tend to be smoothed out.
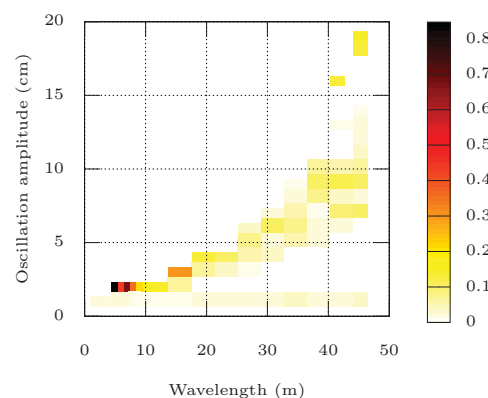

Figure 26. Profile wavelength analysis of the normalised energy use.
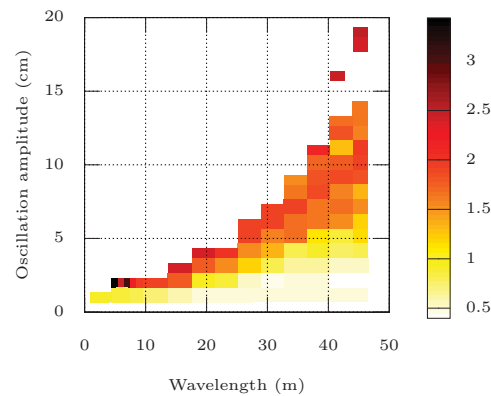
Figure 27. Profile wavelength analysis of the conservative driver discomfort (m/s^2).
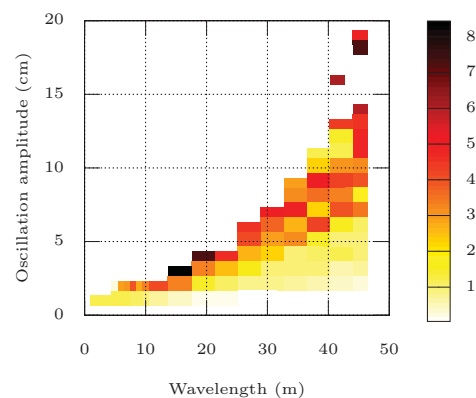
Figure 28. Profile wavelength analysis of the probability than an untrained driver will be sick after 6h on the road (%).

Figure 29. Profile wavelength analysis of normalised suspension wear.

As expected, profile irregularities of greater wavelength require a greater amplitude to affect as strongly the vehicle as a shorter wavelength irregularity would. Moreover, since the wavelength intervals become smaller towards the low end of the wavelength axis, the short wavelength contributions are understated in the graphs shown. In order
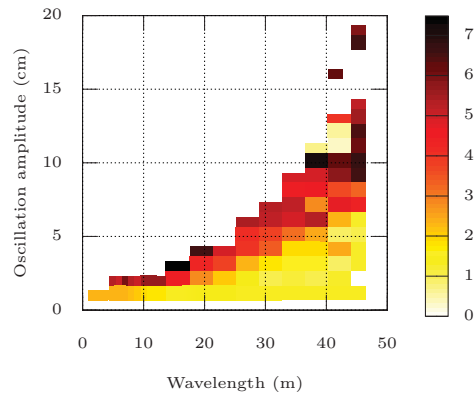
Figure 30. Profile wavelength analysis of normalised tyre wear.

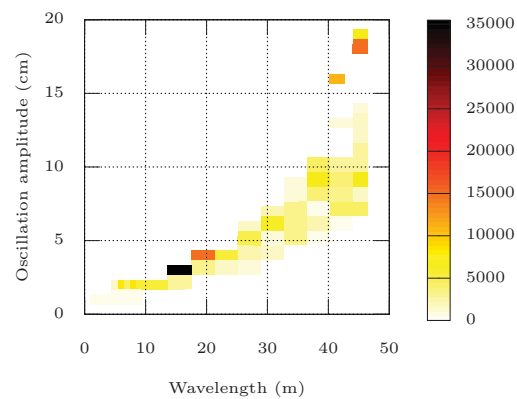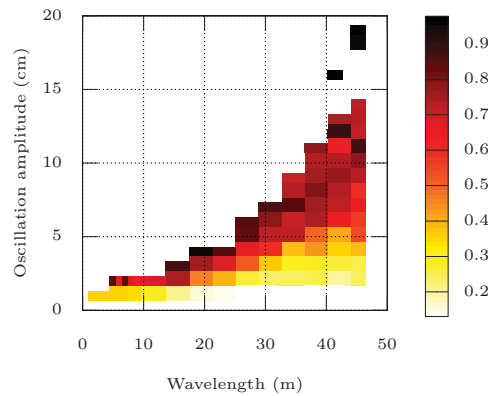Figure 31. Profile wavelength analysis of conservative measure of vibrations likeliness to have an impact on driver health (m/s^2).
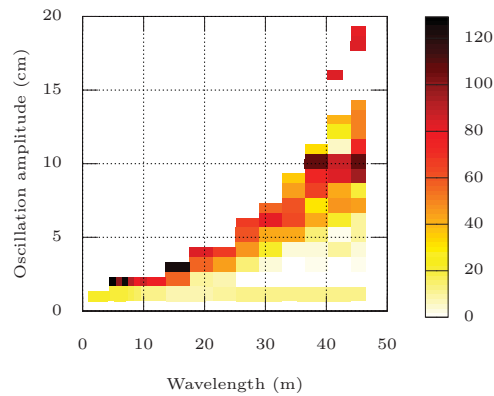
Figure 32. Profile wavelength analysis of safety expressed in average distance (m) by wheel for which the normal force of the non-steering tyres will be lower than 60% of the unperturbed value.

to compare short to medium wavelengths, approximately four adjacent cells of short wavelengths should be added up to obtain the same bandwidth and thus the equivalent probability of impact accumulation. The same reasoning applies between medium and

L. Gagnon, G. Doré, and M. J. Richard

Table 2. Best coefficients of determination obtained for each index presented.

Measured impact	Index	R^2	Degree
Energy	Simple Health index	0.91	1
	Simple Safety index	0.82	1
	Simple Health index	0.91	2
	Simple Safety index	0.78	2
Tyre wear	IRI	0.85	1
	Long waves FRI	0.98	1
Component wear	Four point Health index	0.90	2
	Simple Health index	0.83	1
	Simple Safety index	0.72	2
	Simple Safety index	0.73	1
	FRI	0.47	2
	Four point Wear index	0.73	1
Health	Long waves FRI	0.98	1
	Long waves HRI	0.97	1
	Long waves IRI	0.97	1
	IRI	0.85	1
Safety	Safety index	0.85	1
	Four point Health index	0.89	1
	Four point Wear index	0.72	1
Global impact	IRI	0.78	1

large wavelengths.

Figure 27 agrees quite well with results presented by Richard *et al.* (2009) since wavelengths between 5 m and 20 m visibly have the strongest influence on driver discomfort at the smallest amplitude. Figures 29 and 30 show that large wavelengths may still be present when there is an impact on wear. On Figure 26, one can notice that wavelengths between 4 m and 8 m seem to be the most present when there is a marked impact on energy consumption and this agrees well with the results of Wambold (1985). Figure 28 shows that, as expected, long wavelengths are likely the cause of nausea.

Concerning safety, Figure 32 confirms that medium wavelengths have the most important impact, but do not neglect to show that long wavelengths may be present. The medium wavelengths impact is limited and the short wavelengths impact is negligible. Figure 31 outlines the contribution of long wavelengths to driver health issues and is the only surface plot to show an impact contribution that does not necessarily decrease when wavelengths increase at constant amplitude. This means that a short wavelength perturbation has to repeat itself until it attains the same length as a long wavelength perturbation to provoke the same impact on health.

5.   Conclusion

While the IRI is seen to be a good indicator for the average of all impacts and tyre wear, it is unable to assess the other individual impacts. With the help of the indices hereby presented, it becomes possible to quickly quantify the impact caused by the degradation of a specific road. It is thus recommended to anyone wishing to obtain specific impact contributions to use the indices of Table 2 which gives an overview of the best correlations obtained with the different indices that were examined.

For all indices, component wear is better represented by quadratic correlations than

either linear of higher order ones. The wavelength analysis promises to be a useful tool for quickly evaluating profiles.

The overall conclusions which apply to both parts of the article are that 1) medium wavelengths severely impact fuel consumption, component wear, and safety; 2) simple, two point, and four point indices yield similar results, but the more points the better the correlation; and, 3) the IRI is good at predicting general trends in road-induced vehicular impact but is weak for specific impacts.

Further work could include a more thorough fatigue analysis, examining real profiles that do reach extreme impact and extreme indices, and using the wavelength analysis method to predict and verify profile induced impacts.

Acknowledgement(s)

References

Ahlin, K. and Granlund, N.O.J., 2002. Relating Road Roughness and Vehicle Speeds to Human Whole Body Vibration and Exposure Limits. *International Journal of Pavement Engineering*, 3 (4), 207–216.

Aukland, N., *et al.*, 2003. Frictional work as a sliding wear evaluation parameter. *In: Proceedings of the Forty-Ninth IEEE Holm Conference on Electrical Contacts*, 51–58.

Bogsjö, K., 2006. Development of analysis tools and stochastic models of road profiles regarding their influence on heavy vehicle fatigue. *Vehi Syst Dynam*, 44 (S1), 780–790.

Bogsjö, K., 2007. Evaluation of stochastic models of parallel road tracks. *Probabilistic Engineering Mechanics*, 22 (4), 362–370.

Boresi, A.P. and Schmidt, R.J., 2003. *Advanced mechanics of materials*. 6 John Wiley & Sons.

Breytenbach, B. and Els, P.S., 2011. Optimal vehicle suspension characteristics for increased structural fatigue life. *Journal of Terramechanics*, 48 (6), 397–408.

Cantisani, G. and Loprencipe, G., 2010. Road Roughness and Whole Body Vibration: Evaluation Tools and Comfort Limits. *Journal of Transportation Engineering*, 136 (9), 818–826.

Cho, J.R., Choi, J.H., and Kim, Y.S., 2011. Abrasive wear amount estimate for 3D patterned tire utilizing frictional dynamic rolling analysis. *Tribology International*, 44, 850–858.

Conle, F. and Mousseau, C., 1991. Using vehicle dynamics simulations and finite-element results to generate ffatigue life contours for chassis components. *International Journal of Fatigue*, 13 (3), 195–205.

FAA, Guidelines and procedures for measuring airfield pavement roughness. AC 150/5380-9, Washington, DC, 2009. .

Haiba, M., *et al.*, 2002. Review of life assessment techniques applied to dynamically loaded automotive components. *Computers & Structures*, 80 (5–6), 481–494.

Howe, J.G., *et al.*, 2004. Quarter car model stress analysis for terrain/road profile ratings. *International Journal of Vehicle Design*, 36 (2/3), 248–269.

Jackson, R.L., *et al.*, Synthesis of the effects of pavement properties on tire rolling resistance. , 2011. , Technical report, National Center for Asphalt Technology, Auburn University, Auburn, Alabama.

Jones, T.E. and Robinson, R., A study of the cost-effectiveness of grading unpaved roads in developing countries. , 1986. , Technical report, Transport and Road Research Laboratory, United Kingdom.

Knisley, S., 2002. A correlation between rolling tire contact friction energy and indoor tread wear. *Tire Science and Technology*, 30 (2), 83–89.

Lee, Y.L. and Barkey, M.E., 2012. Metal fatigue analysis handbook : practical problem-solving techniques for computer-aided engineering*In: Stress-based multiaxial fatigue analysis.*, 161–213 Elsevier Science.

Lee, Y.L., Tjhung, T., and Jordan, A., 2007. A life prediction model for welded joints under multiaxial variable amplitude loading histories. *International Journal of Fatigue*, 29 (6), 1162–1173.

Lin, K., *et al.*, 2006. Durability assessment and riding comfort evaluation of a new type scooter by road simulation technique. *SAE Technical Paper*.

Martel, N., St-Laurent, S., and Parent, M., Projet de recherche sur lutilisation des bandes dondes pour lévaluation de luni au Québec. , 2011. , Technical report, Ministère des Transports du Québec.

McLean, J. and Foley, G., Road surface characteristics and condition: effects on road users. , 1998. , Technical report, ARRB Transport Research.

Pitoiset, X., 2001. Méthodes spectrales pour une analyse en fatigue des structures métalliques sous chargements aléatoires multiaxiaux. Thesis (PhD). Université Libre de Bruxelles.

Pitoiset, X., Preumont, A., and Kernilis, A., 1998. Tools for multiaxial fatigue analysis of structures submitted to random vibrations. *In: Proceedings European Conference on Spacecraft Structures Materials and Mechanical Testing*, Braunschweig, Germany.

Pitoset, X., Preumont, A., and Kernilis, A., 1999. Tools for a multiaxial fatigue analysis of structures submitted to random vibration. *In: Proceedings European Conference on Spacecraft Structures, Materials and Mechanical Testing*, Braunschweig Germany.

Poelman, M.A. and Weir, R.P., 1992. Vehicle fatigue induced by road surface roughness. *Vehicle, tire, pavement interface, ASTM STP 1164*. American Society for Testing and Materials, 97–111.

Preumont, A., 1990. *Vibrations aléatoires et analyse spectrale*. Lausanne: Presses polytechniques et universitaires romandes.

Preumont, A. and Piéfort, V., 1994. Predicting random high cycle fatigue life with finite elements. *Journal of Vibration and Acoustics*, 116, 245–248.

Rahman, R.A., Tamin, M.N., and Kurdi, O., 2008. Stress analysis of heavy duty truck chassis as a preliminary data for its fatigue life prediction using fem . *Jurnal Mekanikal*, (26), 76–85.

Rakheja, S., Ahmed, A.K.W., and Stiharu, I., Urban Bus Optimal Passive Suspension Study. , 2001. , Technical report, Concordia University.

Rice, R.C., ed. , 1997. *SAE Fatigue Design Handbook*. Society of Automotive Engineers International.

Richard, M.J., *et al.*, 2009. Étude des conséquences de la détérioration de l'uni des chaussées sur le comportement des véhicules et la sécurité des usagers de la route. *Revue canadienne de génie civil*, 36 (3), 504–513.

Rychlik, I., 1987. A New Definition of the Rainflow Cycle Counting Method. *Int. J. Fatigue*, 9 (2), 119–121.

Saga, M., *et al.*, 2005. Contribution to discrete structural optimisation. *In: 6th International multidisciplinary Conference*.

Savkoor, A.R., 1966. Some aspects of friction and wear of tyres arivisng from deformations, slip, and stresses at the ground contact. *Wear*, 9, 66–78.

Veith, A.G., 1986. The Tire Pavement Interface: A Symposium*In: The most complex tire-pavement interaction: tire wear.*, 125–158 American Society for Testing and Materials.

Wambold, J.C., 1985. Road roughness effects on vehicle dynamics. *Measuring road roughness and its effects on user cost and comfort*. American Society for Testing and Materials, 179–196.

Wetzel, R.M., 1977. *Fatigue under complex loading: analyses and experiments*. SAE.

Yang, X. and Xu, P., 2012. Metal fatigue analysis handbook : practical problem-solving techniques for computer-aided engineering*In: Road load analysis techniques in automotive engineering.*, 1–60 Elsevier Science.

Zaniewski, J.P. and Butler, B.C., 1985. Vehicle operating costs related to operating mode, road design, and pavement condition. *Measuring road roughness and its effects on user and comfort: a symposium*. American Society for Testing and Materials.